

Ultrahigh Precision Machining of Polymer Surface using Laser-Induced Reactive Micro-Plasmas

Leon Streisel, Martin Ehrhardt, Pierre Lorenz, Robert Heinke, Afaque Hossain, and Klaus Zimmer*

*Leibniz Institute of Surface Engineering (IOM), Department of Ultra-precision Surfaces,
Permoserstr. 15, 04318 Leipzig, Germany*

**Corresponding author. E-mail address: klaus.zimmer@iom-leipzig.de*

The process requirements for ultra-precise machining of surfaces for optical applications is still challenging for laser ablation-based methods. The LIPE (laser-induced plasma etching) method combines the two complementary techniques of laser and plasma processing. Technologically important materials like SiO₂, Ge, Si as well fiber-reinforced composites (SiC-SiC) have been successfully processed with LIPE, in particular Polyimide (Kapton@ HN (125 μm)) and Polyethyleneterephthalat. In the present paper, LIPE etching of polymer surface is demonstrated. The influence of the main process parameters on the etching rate as well as on the obtained surface characteristics will be shown and discussed in detail.

DOI: 10.2961/jlmn.2022.01.2005

Keywords: laser, optical breakdown, plasma formation, etching, reactive etching, LIPE, polymer, PET, Kapton

1. Introduction

The investigation and development of processes to enable precise structuring of surfaces with beam-based technologies is an ongoing task. Common methods for precise surface structuring make use of the interaction between the surface and ions [1-3], plasmas [3, 4] or photons [5]. However, dry etching processes based on the interaction between ion beams or plasma and the surface commonly require complex equipment due to the required vacuum condition.

A plasma-based surface structuring process which can be performed at atmospheric pressure is atmospheric pressure plasma-jet processing (APPJ). Surface structuring with APPJ is based on a chemical reaction of the surface atoms with reactive species which are generated inside the plasma. If the chemical reaction results in the formation of volatile products, a steady material removal process can be observed. It was shown that with APPJs a wide variety of materials can be processed [6] and a high surface quality of the processed surface can be achieved [7-9]. Despite this, surface processing with APPJs is limited by the tool size of the plasma jet which is commonly in the range of mm or sub-mm, making the generation of structures smaller than said range challenging.

Another dry etching process which can be performed at atmospheric pressure is laser processing. Laser processing was extensively investigated in the last decade [4, 10-12] and has a wide range of scientific and industrial applications. Laser processing is characterized by a high flexibility and a small footprint in the micrometer range. The interaction of the laser pulses with a surface can result in a material removal. Based on the surface material as well as the characteristics of the laser radiation the material removal process is dominated by different mechanisms. Those include thermally dominated process for e.g., processing of metal using laser pulses with a duration of micro- and nanoseconds [13]. However, using laser radiations with UV wavelengths can

lead to material removal through photothermal [4, 14, 15] and photochemical decomposition [4, 15, 16]. Laser surface structuring based on photochemical decomposition is mainly used by processing of polymers with e.g., excimer laser radiation [4, 17, 18]. These photothermal and photochemical decomposition-based laser processes commonly have a higher surface quality in terms of surface roughness and achievable depth precision in comparison to standard laser ablation. Yet, even by using UV-laser radiation the achievable depth precision per applied laser pulse is usually limited by the absorption length of the used laser wavelength in the surface material. Typical ablation rates achieved by laser processing are in the range of 10 to 100 nm/pulse. Particularly laser radiation of polymer surfaces has been discussed in several studies before [19, 20], which demonstrated the viability and limitations as well as possible applications in biophysics and medicine. The combination of laser processing with plasma etching at atmospheric pressure is a new approach for ultra-precise surface structuring.

The so called LIPE (Laser Induced Plasma Etching) is based on a micro-plasma ignited by a laser induced optical breakdown. The generated plasma is the source of reactive species, which can interact with a surface and result in chemical etching given a sufficiently small distance between the plasma and the surface. It was shown in previous studies that materials like SiO₂ [21], Ge [22], Si [23] and SiC-SiC composites [24] can be processed using LIPE. The achieved surface quality was high with e.g., a measured surface roughness of < 2.4 nm rms [22] and 1.4 nm rms [21] for Ge and SiO₂ respectively. It was found that the material removal depth per applied laser pulse is on average one atomic layer which makes the LIPE process suitable for ultra-precise surface structuring.

In the present study LIPE processing of polymer surfaces will be investigated. The freestanding micro plasma is generated by ultrashort laser pulses (150 fs, 775 nm). The etching experiments will be performed in air or in oxygen at

atmospheric pressure. As substrate material Polyimide (Kapton@ HN (125 μm)) and PET will be used. Polyimide is a high-sought after material in current industrial processes, due to their flexibility and properties. Applications range from semiconductors, high temperature plastics, membranes to aerospace, optoelectronics and microelectronics. LIPE characteristics are investigated in dependence of the etching time, the distance of the plasma and the substrate surface, the laser pulse energy, the etching gas, the substrate temperature and the to be etched material. The morphology of the generated etching grooves will be investigated via white light interferometry (WLIM).

2. Experimental Setup

The experimental setup comprises of a laser and a substrate chamber. A sketch of the experimental setup can be seen in Fig. 1.

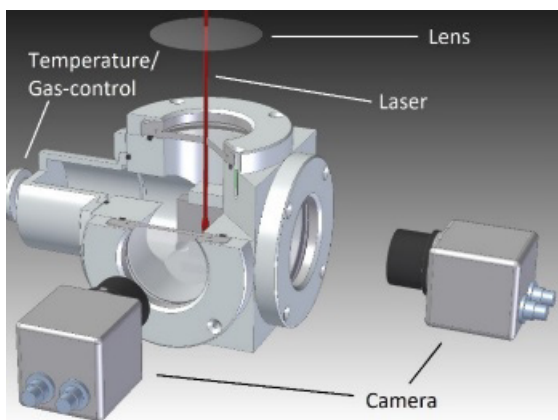


Fig. 1 Sketch of the experimental Setup

The laser has the following properties: Its pulse duration is 150 fs, the pulse repetition rate is 1 kHz, the used wavelength is 775 nm and the maximum pulse energy is 1 mJ. The laser pulse energy can be adjusted with a polarizing beam splitter. The beam is guided by several mirrors to the top of the etching chamber and focused by 60 mm focal distance lens, before entering the chamber through a window. Due to the optical breakdown which occurs at the focal point when the pulse energy is high enough, a laser-induced plasma is created inside of the chamber which can be seen in Fig. 2.

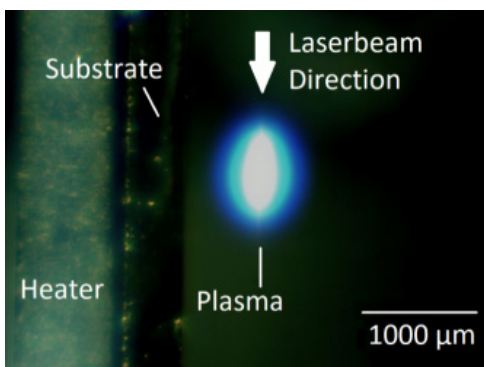


Fig. 2 Camera-generated Image of the laser induced plasma (LIP) inside the experimental chamber

The chamber itself is fixed upon a movable X-Y-Z stage which is controlled by a computer with a precision of $\sim 1 \mu\text{m}$. The chamber can furthermore be tilted regarding the laser path, aligning the sample surface parallel to it. The inside volume of the chamber is around 400 cm^3 , which compares to an estimated plasma volume of less than 10 mm^3 . The plasma and the substrate inside the chamber can be observed with two cameras, which monitor the plasma in real time. The cameras are angled at 90° to each other and view the plasma through side windows. The positions of each camera can be freely adjusted. Due to their resolution the distance between the plasma and the substrate surface can be adjusted with a precision of $\sim 5 \mu\text{m}$ when measuring the distance between the plasma and the substrate. Said distance was measured from the surface of the substrate to the center of the plasma in all future mentions.

Three metal clips fix the position of the substrate on top of the heater inside the chamber. The heater is controlled externally and can be accessed via two electrodes on the outside of the chamber. Additionally, the chamber features a gas feed and a pressure control unit. This allows for a constant gas flow which guarantees a stable pressure inside the chamber. The gas flow rates when used were 667 sccm under AT conditions. Air and oxygen were chosen to function as etching gas. The sample materials to be etched were polyimide (Kapton@ HN (125 μm)) and Polyethylenterephthalat (PET). They were cut into pieces of $\sim 10 \text{ mm} \times 10 \text{ mm}$. The samples were used as received without further surface cleaning. After the etching, the samples were analyzed by a white light interference microscope (NPFLEX, Bruker).

Before the start of the etching process, the laser induces a plasma inside the chamber with a pulse energy high enough to induce optical breakdown. After locating the plasma with the two cameras, the substrate is moved by the translation-stage. Once the desired distance between the center of the plasma and the surface of the substrate is acquired, the etching process begins.

3. Results

The interaction between the laser-induced micro plasma and the polymer substrate amounts to changes in the surface of the used polymer. According to the position of the plasma, the formation of grooves can be observed.

Fig. 3 shows the properties of an example groove as measured with WLIM. Both the cross-section in Y and in X direction display the characteristic shape of the groove, as well as showing asymmetry for the Y-axis. The Contour plot also shows the difference in the length of the groove between the two axes, with it being longer in the direction of the path of the laser beam. For the shown exemplary groove in Fig. 3 the groove itself has a size of $\sim 120 \mu\text{m} \times 190 \mu\text{m}$, for the X and Y axes respectively. The shape and morphology of the etching groove did not change significantly over the course of any of the measurements, however the size of the etching groove differs from the laser spot size in the focal plane which is circular and has a radius of $\sim 7 \mu\text{m}$.

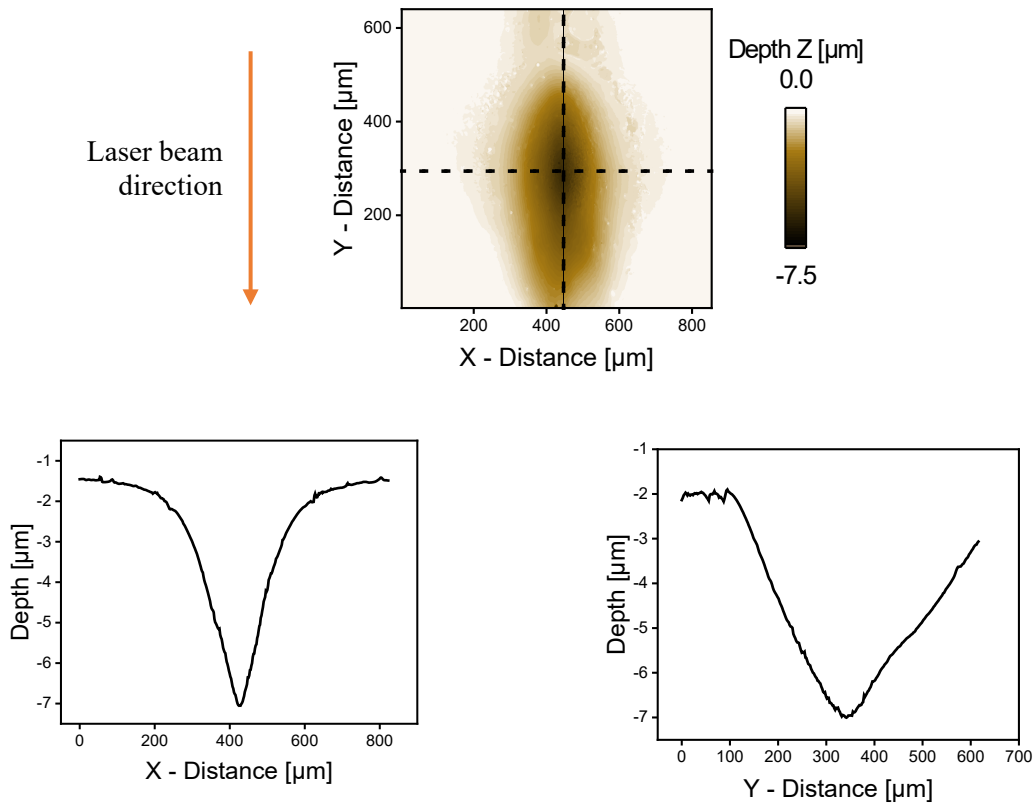


Fig. 3 Contour plot of an exemplary etching groove measured with a white light interferometer (upper image). Cross sections of the etching groove along the dotted lines in x-direction (left) and y-direction (right).

In Fig. 4, the dependence of the cumulative etching depth on the etching time is plotted. It can be observed that by increasing the etching time the depth of the groove increases, up to a maximum etching depth of 15.5 μm after 15 min of etching. The slope of the graph is slightly flattening with increasing etching time.

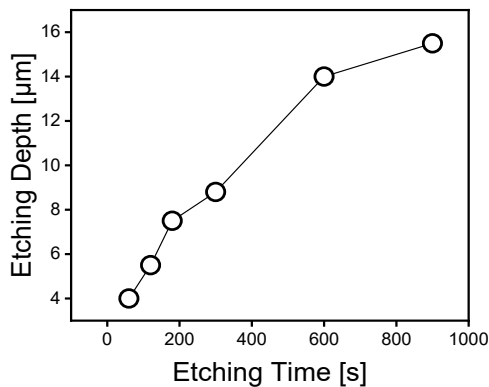


Fig. 4 The cumulative etching depth in dependence of the etching time for a pulse energy of 660 μJ , an etching time of 180 s, with a substrate at RT. Air was used as etching gas at atmospheric pressure. Kapton@ HN was used as substrate material.

The relation between etching rates and etching time are shown in Fig. 5. The etching rates were determined by dividing the corresponding maximum depth of the groove by

the etching time. Therefore, the calculated result is an average etching rate. In addition to the etching rate per time, Fig. 5 shows the etching rate per applied laser pulse. The number of applied laser pulses was calculated considering the laser pulse repetition rate of 1 kHz. It can be gathered from the graph that with increasing the etching time the etching rate decreases. The maximum etching rate of $\sim 67 \text{ nm/s}$ was measured at an etching time of 1 min. The minimum etching rate of $\sim 17 \text{ nm/s}$ was measured at an etching time of 15 min.

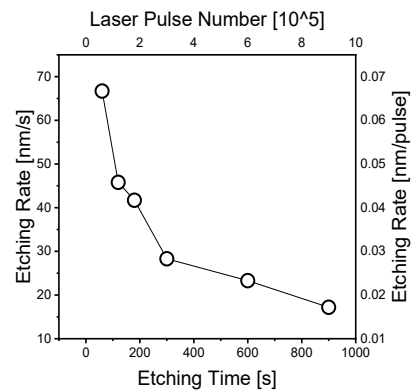


Fig. 5 Etching rate in dependence of etching time for a laser pulse energy of 660 μJ , an etching distance of 100 μm , with a substrate at RT. Air was used as etching gas at atmospheric pressure. Kapton@ HN was used as substrate material.

In the graph shown in Fig. 6, the dependence of the etching rate on the etching distance between the center of the plasma and the substrate is demonstrated. It ranges from 80 μm to 200 μm . As shown by the graph, the correlation is inverse: The smaller the distance, the higher the etching rate. It can also be gathered, that by using the maximum plasma-surface distance of 200 μm an etching of the surface was not totally prevented. Due to the experimental setup, it was not possible to shorten the distance further, without leaving traces of direct ablation from the laser beams onto the polymer.

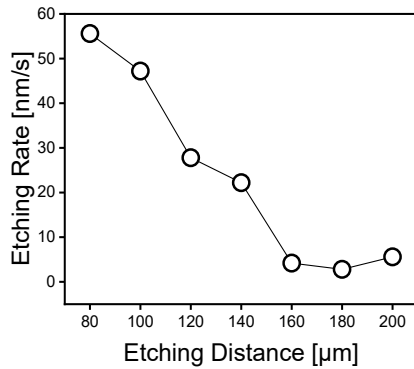


Fig. 6 Etching rate in dependence of etching distance for a laser pulse energy of 693 μJ , a time of 180 s, with a substrate at RT. Air was used as etching gas at atmospheric pressure. Kapton@ HN was used as substrate material.

In Fig. 7 the influence of varying the laser pulse energy on the etching rate is shown. In contrast to the distance, increasing the pulse energy leads to higher etching rates, with a maximum of 75 nm/s at the highest power of 774 μJ . The increase is monotone.

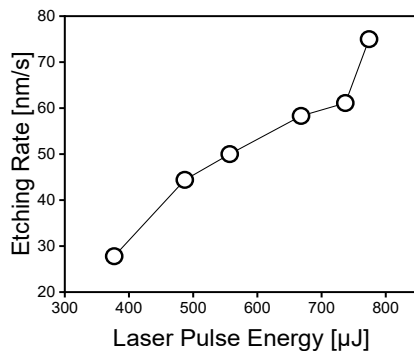


Fig. 7: Etching rate in dependence of laser pulse energy for an etching distance of 100 μm , a time of 180 s, with a substrate at RT. Air was used as etching gas at atmospheric pressure. Kapton@ HN was used as substrate material.

The difference in using oxygen instead of air as the etching gas is displayed in Fig. 8. For both measurements, the same parameters were used to allow for direct comparison. As seen in the graph, both conditions lead to the same shape of correlation between time and etching rate.

However, the etching rates when using oxygen are without exception higher for all points measured. This difference in etching rate ranges from 83 nm/s to 32 nm/s. The difference between the two values diminishes at increased etching times.

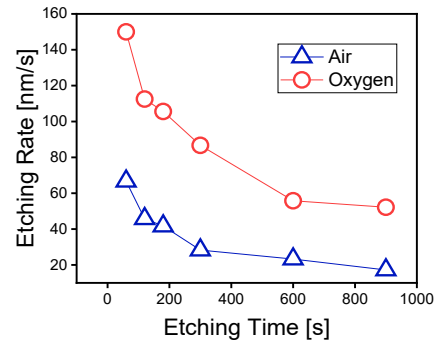


Fig. 8 Etching rate in dependence of etching time for a laser pulse energy of 774 μJ , an etching distance of 100 μm , with a substrate at RT. Air (blue) / oxygen (red) was used as etching gas at atmospheric pressure. Kapton@ HN was used as substrate material.

Fig. 9 explores the change in etching rate when varying the temperature of the sample. It can be seen in the graph, that the etching rate increases when increasing the temperature. The highest etching rate of 247 nm/s was achieved at a temperature of 525 K. For lower values of temperature, the increase in etching rate appears to grow linearly.

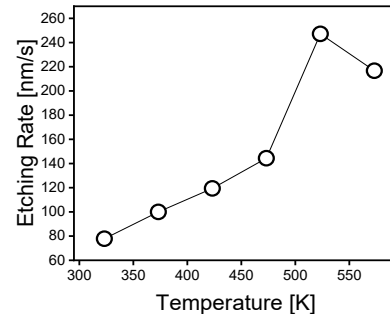


Fig. 9 Etching rate in dependence of temperature for a laser pulse energy of 774 μJ , an etching time of 180 s and an etching distance of 100 μm . Air was used as etching gas at atmospheric pressure. Kapton@ HN was used as substrate material.

Two materials were chosen and compared to each other, namely Kapton@ HN (125 μm) and Polyethylenterephthalat (PET). The results are shown in Fig. 10. Both samples shared the same parameters across the several measurement points. PET has higher etching rates than polyimide across the entire etching time range. The difference ranges from 133 nm/s to 38 nm/s. The time of the highest and lowest etching rate for each material is the same at 1 min and 15 min respectively. Similarly, the trend of diminishing etching rates for larger times is shared.

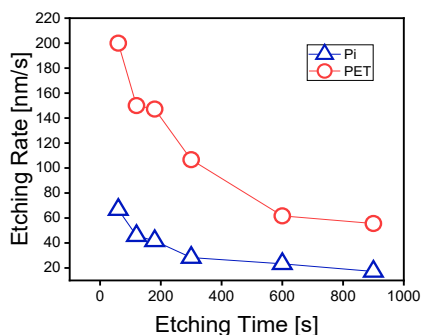


Fig. 10 Etching rate in dependence of etching time for a laser pulse energy of 751 μJ , an etching distance of 100 μm , with a substrate at RT. Air was used as etching gas at atmospheric pressure. Kapton@ HN (blue) / Polyethylenterephthalat was used as substrate material.

4. Discussion

Etching experiments on polyimide and PET were conducted using a laser-ignited plasma with air and oxygen as etching gas. Plasma etching of polymer surfaces with air or oxygen as etching gas comprise of various chemical and physical processes which have been analyzed in detail in numerous previous studies [25-29]. Thus, the present paper will not give a detailed description, but rather give a summarizing overview as well as an evaluation of the importance of the different mechanisms.

The etching process starts with the formation of reactive species due to the laser-induced plasma. The reactive species will then diffuse to the substrate surface and react, leading to the creation of volatile products. These will then detach and diffuse away from the surface. Due to the experimental setup additional material removal due to laser ablation can be excluded. This is further proven by the differences in size between the laser spot and the etching groove shape and the low etching rate seen in Fig. 5. Similarly, due to the pressure and distance of the plasma to the substrate surface, the influence of ion or electron bombardment causing sputter effects can be neglected, given a mean free path length of ~ 100 nm in atmospheric pressure. This combined results in a chemical etching process-dominated material removal of the surface, which is supported by the observed morphology of the etching groove under WLIM. Since the etching gas in use was either air or pure oxygen, the reactive species majorly consist of atomic oxygen. The addition of reactive nitrogen species may give rise to direct etching of the polymer used [30]. The resulting gaseous products of the interaction of reactive species with the polymer are mainly CO, CO₂, H₂O, H₂ and N₂ [29, 31], which can condensate and form deposits on the surface outside the etching groove. The influence of UV and X-ray radiation generated during the optical breakdown can support the etching process [32-34].

The plasma enabling the etching process was generated by an optical breakdown. An optical breakdown can be defined as achieving an electron density of $\sim 10^{14}$ cm⁻³ [35]. After reaching the corresponding threshold for the power density, a sharp increase in electron density can be observed. There are two main processes for electron generation, multiphoton ionization (MPI) and avalanche ionization (AI). A detailed explanation can be found in [36] [4, 37]. In a previ-

ous study, the same configuration led to a threshold for generation a visible plasma of 200 μJ [21]. The influence of the laser pulse energy on the etching rate is a positive, given the increase in etching rate when increasing the laser pulse energy, as shown in Fig. 7. The exact mechanisms behind this exact dependence are most probably caused by a combination of processes which are not yet fully understood. However, the general trend of an increase in etch rate when increasing the laser pulse energy can be explained by an increase in plasma volume which leads to an increase in the number of reactive species and a shorter path to the surface. Additionally, a higher energy density amplifies the generation of reactive species through higher electron density and temperature.

In Fig. 5, it can be seen that the etching rate decreases with etching time. This is a typical seen effect [22], which can be attributed to a geometric factor, namely the increase in etching distance between the plasma and the substrate surface due to a larger etching depth at higher etching times. This leads to an increase in diffusion length and diffusion time which decreases the average density of reactive species at the surface of the substrate. This effect can be seen in Fig. 6, and roughly follows a linear dependence. The highest measured absolute etching rate value of 67 nm/s for polyimide compares to 66 nm/s for germanium [22]. Although the etching rate values are very similar, the corresponding etching time for Ge is 2 min, whereas for polyimide the highest etching rate was measured for an etching time of 1 min [22]. These differences are a result of the difference in chemical interactions with the substrate, since in previous studies a mixture of CF₄ and O₂ was used as etching gas and germanium was used as substrate.

From the investigations with the WLIM the surface in the etching groove is rather smooth however in the outer regions, impurities can be found. Those impurities as seen in the contour plot of Fig. 3 are likely to be deposits of volatile products of surface etching which have condensed and diffused back onto the surface. This is, however, only an assumption and should be further investigated with other measurements, such as XPS (X-ray photoelectron spectroscopy).

The increase of etching rate with increasing substrate temperature (Fig. 9) is a direct consequence of increasing chemical reaction rates at the substrate. A higher frequency of reactions leads to a larger material loss and in turn etching rate.

The dependence of the etching rate on the choice of etching gas (Fig. 8) is in line with expectations. This is because a higher concentration of oxygen leads to a higher density of reactive species, namely atomic oxygen, inside the plasma. Since the diffusion process is similar for both choices of etching gas, this also increases the density of reactive species at the surface of the substrate. Because a higher density leads to more frequent formations of volatile products and thus material loss, an increase in oxygen concentration is followed by an increase in etching rate.

The difference in etching rate between different polymers was exemplary measured in Fig. 10. As expected, the shape of the graphs is the same, which is in accordance with the similarity in their chemical structure. The noteworthy higher values for PET range from an increase of 130 % to 40 % when compared to Kapton@ HN (125 μm), depending

on the chosen etching time. When comparing the results to other studies [25], their increase ranges from 50 % to 120 % increase, which is in line with the data from this study. This difference could be explained by the difference in temperature resistance which would explain the higher etching rate of PET, as well as its higher flattening in comparison to Kapton@ HN (125 μm), since the temperature of the substrate decreases with greater distance from the plasma.

In conclusion, the etching rate and in consequence etching depth of polymers with a laser-induced plasma can be precisely controlled, due the strong and mostly linear dependence of numerous parameters as well as the low etching rate itself, which allows for precise surface structuring.

5. Summary

This paper has demonstrated the high-quality machining of polyimide using a laser-induced plasma under various conditions as well as their influence on the etching process. This was done with a laser pulse duration of 150 fs, a pulse repetition rate of 1 kHz and a wavelength of 775 nm. Focusing of the laser beams led to an optical breakdown in a reactive gas mixture causing their activation and allowing dry etching of the substrate. The pressure of the chamber was kept at atmospheric conditions, and the gas inside was either air or pure oxygen, with oxygen increasing the etching effect. The precision of this method is shown by the average etching depth per laser pulse of $< 1 \text{ \AA}$. Since the distance between the substrate and the plasma increases with greater etching depth, this likely explains the decrease in etching rate over time. The etching rate increased linearly with the pulse energy and temperature but decreased linearly with plasma - substrate distance. Pure oxygen as etching gas showed a much higher etching rate than air. Altogether, it has been shown that the method of dry etching can be used on polyimide and allows for precise etching of its surface.

Acknowledgements

The work was funded by the Deutsche Forschungsgemeinschaft (DFG, German Research Foundation) – No. 392226212 and No. 453925455.

References

- [1] D. Fink, P. Alegaonkar, A. Petrov, M. Wilhelm, P. Szimkowiak, M. Behar, D. Sinha, W. Fahrner, K. Hoppe and L. Chadderton: Nucl. Instrum. Meth. B, 236, (2005) 11.
- [2] J.J. Cuomo, S.M. Rosnagel, and H.R. Kaufman: "Handbook of ion beam processing technology", (N. p., United States, 1989).
- [3] A. Schindler, T. Haensel, D. Flamm, W. Frank, G. Boehm, F. Frost, R. Fechner, F. Bigl, and B. Rauschenbach: Proc. SPIE, Vol. 4440, (2001) 4440217.
- [4] D. Bäuerle: "Laser Processing and Chemistry", (Springer, Berlin, Heidelberg, New York, 2011).
- [5] T. Lippert, Plasma. Process. Polym., 2 (2005) 525.
- [6] G. Selwyn, H. Herrmann, J. Park, and I. Henins: Contrib. Plasm. Phys., 41, (2001) 610.
- [7] O.V. Penkov, M. Khadem, W.-S. Lim, and D.-E. Kim: J. Coat. Technol. Res., 12, (2015) 225.
- [8] F. Kazemi, T. Arnold, P. Lorenz, M. Ehrhardt, and K. Zimmer: Appl. Surf. Sci., 551, (2021) 149339.
- [9] F. Kazemi, T. Arnold, P. Lorenz, M. Ehrhardt, and K. Zimmer: Plasma. Chem. Plasma. P., 40, (2020) 1241.
- [10] J.D. Majumdar, and I. Manna: Sadhana, 28, (2003) 495.
- [11] R. Crafer, and P.J. Oakley: "Laser processing in manufacturing", (Chapman & Hall, London, New York, 1993).
- [12] G. Yang: "Laser ablation in liquids", (Jenny Stanford Publishing, New York, 2012.).
- [13] K.-H. Leitz, B. Redlingshöfer, Y. Reg, A. Otto, and M. Schmidt: Physcs. Proc., 12, (2011) 230.
- [14] S.R. Cain, F. Burns, C.E. Otis, and B. Braren: Jpn. J. Appl. Phys., 72, (1992) 5172.
- [15] E. Akman, Y. Erdoğan, M.Ö. Bora, O. Çoban, B.G. Oztoprak, and A. Demir: Int. J. Adhes. Adhes., 98, (2020) 102548.
- [16] M. Day, and D. Wiles: J. Appl. Polym. Sci., 16, (1972) 191.
- [17] P. Dyer, Excimer laser polymer ablation: twenty years on, Applied Physics A, 77, (2003) 167-173.
- [18] J. Wei, N. Hoogen, T. Lippert, O. Nuyken, and A. Wokaun: J. Phys. Chem. B, 105, (2001) 1267.
- [19] T.G. Volova, A.A. Tarasevich, A.I. Golubev, A.N. Boyandin, A.A. Shumilova, E.D. Nikolaeva, and E.I. Shishatskaya: J. Biomat. Sci.-Polym. E., 26, (2015) 1210.
- [20] T.G. Volova, A.I. Golubev, I.V. Nemtsev, A.V. Lukyanenko, A.E. Dudaev, and E.I. Shishatskaya: Polymers-Basel, 13, (2021) 1553.
- [21] M. Ehrhardt, P. Lorenz, B. Han, and K. Zimmer: APPL Phys. A-Mater., 126, (2020) 1.
- [22] M. Ehrhardt, P. Lorenz, J. Bauer, R. Heinke, M.A. Hossain, B. Han, and K. Zimmer: Lasers Manuf. Mater. Process., (2021) 1.
- [23] R. Heinke, M. Ehrhardt, P. Lorenz, and K. Zimmer: Appl. Surf. Sci. Advances, 6, (2021) 100169.
- [24] K. Zimmer, M. Ehrhardt, P. Lorenz, X. Wang, P. Wang, and S. Sun: Ceram. Int., 48 (2022) 90.
- [25] M.A. Golub, and T. Wydeven: Polym. Degrad. Stabil., 22, (1988) 325.
- [26] L. Yang, J. Chen, Y. Guo, and Z. Zhang: Appl. Surf. Sci., 255, (2009) 4446.
- [27] S.J. Pearton, and D.P. Norton: Plasma Process. Polym., 2, (2005) 16.
- [28] H. Gokan, S. Esho, and Y. Ohnishi: J. Electrochem. Soc., 130, (1983) 143.
- [29] G. Turban, and M. Rapeaux: J. Electrochem. Soc., 130, (1983) 2231.
- [30] G. Smolinsky, E. Truesdale, D. Wang, and D. Maydan: J. Electrochem. Soc., 129, (1982) 1036.
- [31] H.K. Yasuda: "Plasma polymerization", (Elsevier Science, Oxford, 1985).
- [32] J. Guillet: "Polymer Photophysics and Photochemistry", (Cambridge University Press, Camebridge, 1985).
- [33] N.S. Allen: Photochemistry, 34, (2007) 197.
- [34] S.L. Murov, I. Carmichael, and G.L. Hug: "Handbook of photochemistry", (CRC Press, Boca Raton London New York, 1993).
- [35] W. Hu, Y.C. Shin, and G. King: Appl. Phys. Lett., 99, (2011) 234104.
- [36] P. Pronko, P. VanRompay, C. Horvath, F. Loesel, T. Juhasz, X. Liu, and G. Mourou: Phys. Rev. B, 58, (1998) 2387.

- [37] A. Vaidyanathan, T. Walker, and A. Guenther: *Ieee J. Quantum Elect.*, 16, (1980) 89.

(Received: February 7, 2022, Accepted: June 11, 2022)